ACS Biomaterials SCIENCE & ENGINEERING
Cite This: ACS Biomater. Sci. Eng. 2019, 5, 4739−4749
Article
pubs.acs.org/journal/abseba

# Nitrogen-Doped Carbon Quantum Dots for Preventing Biofilm Formation and Eradicating Drug-Resistant Bacteria Infection

Huajuan Wang,[†,‡] Zhiyong Song,[†,§] Jiangjiang Gu,[§] Shuojun Li,[§] Yang Wu,[⊥] and Heyou Han*[,‡,§,⊥]

[‡]State Key Laboratory of Agricultural Microbiology, College of Food Science and Technology, [§]State Key Laboratory of Agricultural Microbiology, College of Science, and [⊥]State Key Laboratory of Agricultural Microbiology, College of Life Science and Technology, Huazhong Agricultural University, No. 1 Shizishan Street, Hongshan District, Wuhan, Hubei China

Supporting Information

**ABSTRACT:** The development of novel antimicrobial agents is a top priority in the fight against drug-resistant bacteria. Here, we synthesized a green nanoantibiotic, nitrogen-doped carbon quantum dots (N-CQDs) from bis-quaternary ammonium salt (BQAS) as carbon and nitrogen sources. The as-obtained N-CQDs possess high antibacterial activity (>99%) against both methicillin-resistant *Staphylococcus aureus* (MRSA) and Ampicillin-resistant *Escherichia coli* bacteria in vitro than some known clinical antibiotics (vancomycin and gentamicin). The N-CQDs can kill MRSA pathogens without inducing resistance, prevent biofilm formation and eliminate established biofilm and persister cells. The treatment of N-CQDs can significantly reduce the amount of bacteria on the infected tissue and accelerate wound healing. The N-CQDs are positively charged, thus enabling them to interact with bacterial cell membrane through electrostatic interaction, leading to severe damage and an increased permeability of the cell membrane, which further promotes the penetration of N-CQDs into the membrane and induces the degradation of DNA by N-CQDs generated reactive oxygen species. The N-CQDs also play a role in obstructing the intracellular metabolic pathways of MRSA. The overall data demonstrate the green nanoantibiotic as an excellent eradicator of biofilm and persister cells as well as a promising antibacterial candidate for treating infections induced by drug-resistant bacteria.

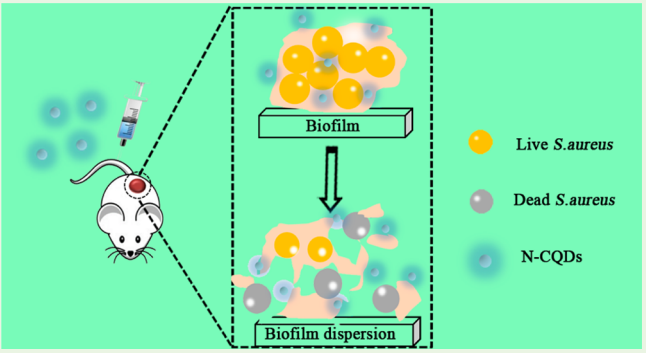


**KEYWORDS:** *green nanoantibiotic, nitrogen-doped carbon quantum dots, drug-resistant bacteria, biofilms, antibacterial mechanism*

## INTRODUCTION

The escalating crisis of multidrug resistance is raising fears that untreatable infections may kill substantial numbers of patients. Furthermore, bacterial infections often take place in biofilm forms with bacteria embedded within a self-produced matrix of extracellular polymeric substances (EPS).[1] The EPS, which possesses a complex composition, architecture, and dynamic function, acts as a barrier to antimicrobial agents, the common antibiotics, which generally eliminate metabolically active planktonic bacteria, may be as much as 1000-fold less potent against biofilm-encased bacteria.[2] What's more, as the antibiotics are deactivated in the EPS matrix more rapidly than they diffuse, penetration can be profoundly retarded.[3] Complete eradication of biofilms requires efficient penetration and accumulation of antimicrobial agents into the biofilm network. The limited penetration depth of antimicrobial agents into biofilms is a huge challenge for treating drug-resistant bacterial infections.[4]

As conventional antibiotics are not effective in treating infections caused by drug-resistant bacteria, the development of novel antimicrobial agents is a top priority in the fight against such bacteria and persistent bacteria.[5−7] Unfortunately, the development of new antibacterial drugs is not as fast as the development of microbial pathogens in resistance, and the investment in the development of new antibacterial drugs is also limited,[8] suggesting the necessity to develop alternative methods to combat bacterial diseases and drug resistance. Recently, to solve the aforementioned problems, several strategies have been proposed, such as small molecules, antimicrobial peptides (AMPs), and drug combination.[9−11] Among these methods, the use of multiple therapeutic agents in combination has become the primary strategy to treat drug-resistance-related diseases. It contains the advantages of the following aspects, synergistic antibacterial effect of drugs to improve efficacy, delay or reduce the emergence of drug-resistant bacteria, combined cases can expand the antibacterial range and reduce individual drug doses, thereby reducing side effects.[12−14] Besides, some nanomaterials with the activity of killing bacteria are considered as nanoantibiotics for treating bacterial infections due to their unique characteristics. Studies have shown that some nanomaterials can damage bacteria directly instead of targeting a specific stage in their metabolic

Received: April 28, 2019
Accepted: July 15, 2019
Published: July 15, 2019






DOI: 10.1021/acsbiomaterials.9b00583
ACS Biomater. Sci. Eng. 2019, 5, 4739−4749

pathways.[15] However, all these antibacterial materials need to improve their performance in a certain area, such as production cost, processing, preservation, and environmental protection. For example, metal and metal oxide nanoparticles are common antibacterial materials and possess good activity against bacteria,[16,17] but the use of metal or metal oxide nanomaterials has raised the concern about their harm to human health or the environment. Hence, the use of metal-free nanomaterials in treating bacteria, especially multidrug-tolerant bacterial cells, has attracted wide attention.

Carbon quantum dots (CQDs), a new type of carbon-based zero-dimensional nanomaterial that appeared in 2004,[18] are composed of dispersed spherical carbon particles with an extremely small size (<10 nm) and belong to a novel nanocarbon material with fluorescent properties. Because of their small particle size, high-aqueous solubility, low toxicity, wide range of raw materials, good biocompatibility, low cost, simplicity in preparation, and ease of functionalization,[19,20] CQDs have attracted much attention from researchers and have been widely used in many fields, such as bacterial sensing, bioimaging, photocatalysis, photodynamic therapy, and antibacterial antimicrobial.[21,22] Unlike metal nanoantibacterial materials, CQDs, a metal-free nanomaterial with carbon as the main component, are environmentally friendly and would not induce the pollution to the environment. In this sense, CQDs can be considered as a green nanoantibiotic.

Interactions between antimicrobial agents and biofilm are crucial in determining the efficacy of treatment. In recent studies, the nanomaterial/biomolecule interfaces can be controlled using electrostatic, hydrophobic, or other noncovalent interactions by surface functionalization, which providing a potential powerful tool for permeating biofilm EPS barrier.[23] Previous studies have shown that neutral and anionic QDs cannot penetrate or accumulate efficiently into biofilms. In contrast, cationic particles readily penetrate fully into biofilms.[24] In this study, the bis-quaternary ammonium salt was employed as a carbon and nitrogen source to prepare water-soluble N-CQDs through a green and facile hydrothermal method in one pot as displayed in Scheme 1, and the

**Scheme 1. Synthesis Route of N-CQDS**

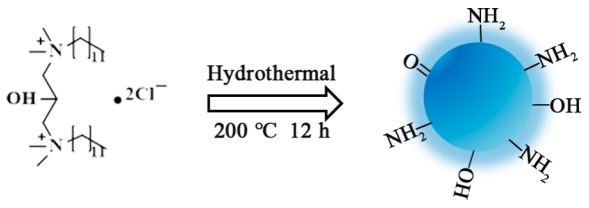


as-prepared N-CQDs are demonstrated to have an excellent activity against drug-resistant bacteria (Scheme 2). More importantly, the N-CQDs can eradicate biofilm and kill the persisters effectively. The antibacterial mechanism of N-CQDs was also explored in detail.

## EXPERIMENTAL SECTION

**Materials.** Vancomycin (Van), penicillin (Pen), and 3-(4,5-dimethylthiazol-yl)-2,5-dimethylthiazol-2-yl)-2,5diphenyltetrazolium bromide (MTT) were purchased from Aladdin. Cytotoxicity Detection Kit$^{PLUS}$ (LDH) was purchased from Roche. Enhanced BCA Protein Assay Kit, propidium iodide (PI), and 4′-6-diamidino-2-phenylindole (DAPI) were obtained from Beyotime Institute of Biotechology (Shanghai, China). Crystal violet was provided from Biosharp.

**Synthesis and Characterization of N-CQDs.** The N-CQDs were prepared by heating Bis-Quaternary ammonium salt (BQAS). Briefly, 0.139 g of BQAS was mixed with 5 mL ultrapure water (Milli-Q, Millipore, 18.2 MU resistivity). After that, the suspension was transferred into a Teflonlined autoclave chamber (20 mL) and heated at 200 °C for 12 h (Figure S1). When finished, the obtained solution was dialyzed through a membrane against ultrapure water for 24 h to clear away the free low molecular weight byproducts (MWCO, 500 Da). The obtained N-CQDs were stored at 4 °C for further use. The particle size of N-CQDs were determined by high-resolution transmission electron microscopy (HRTEM, TEM-2100F, 200 kV, JEOL): took a drop of N-CQDs suspension, then dropped on the copper grid, and observed by HRTEM. The dispersibility of N-CQDs suspension was examined by dynamic light scattering (DLS, Malvern Zetasizer Nano ZS90): dispersed N-CQDs powder into water to form a homogeneous solution, adjusted the concentration to 10 μg/mL, and then took 200 μL of the obtained N-CQDs suspension into the measuring pool, then measured by DLS. In addition, the stability of N-CQDs was evaluated by measuring the particle size at times points of 1, 3, 5, and 7 days. The surface functional groups were determined using Fourier transform infrared spectroscopy (FT-IR, Nicolet Avatar-330 spectrometer).The fluorescence spectra of N-CQDs were obtained with a fluorescence spectrophotometer. Besides, we analyzed the bulk composition of N-CQDs. Brifely, we first prepared the N-CQDs suspension (>6 mL), then used the elementary analyzer-stable isotope ratio mass spectrometers to (EA-IRMS, Elementar Vario PYRO cube, and Isoprime100) to dectect the samples of N-CQDs.

**Bacterial Culture and Assays.** Methicillin-resistant *Staphylococcus aureus* (MRSA)(1213P45A) were isolated from nasal swabs of clinical pigs, ampicillin-resistant *Escherichia coli* (PCN033) were isolated from clinical symptoms of pigs brain tissue. The bacteria were cultured in Luria−Bertani broth medium (LB) Lysogeny Broth (LB) media. Briefly, a single colony of MRSA and Ampicillin-resistant *E. coli* were selected separately from the LB agar plate, followed by incubation in 20 mL of LB culture medium at 30 °C for 12 h under a rotation of 120 r/min. The concentration of bacteria was determined at an optical density of 600 nm ($OD_{600}$).

**Antibacterial Test.** The antimicrobial activity of the N-CQDs was tested by the measurement of $OD_{600}$ and the colony count method. Briefly, 200 μL bacterial suspensions ($10^8$ CFU/mL) were centrifuged, then incubated with a series of concentrations (0, 0.625, 1.25, 2.5 5, and 10 μg/mL) of N-CQDs for 3 h at 30 °C, followed by diluting 10 000 times. Next, taking 20 μL of the diluted suspension spread on the LB agar plates and then cultured at 30 °C for 24 h. Finally, the number of bacterial colonies was counted to display the antibacterial activity.

The minimal inhibitory concentration (MIC) of N-CQDs and antibiotics was examined by the microdilution method as previously reported.[25] Briefly, the experiment was performed in a transparent 96-well plate. N-CQDs and antibiotics were grouped first, with the highest concentration of the relative material (200 μL) in the first well of every group. The remaining wells of each group were supplemented with 100 μL LB medium. Then, 100 μL solution was transferred from the first well of each group to the next one and mixed thoroughly, and the concentration of materials was 2-fold diluted. Double dilution was performed for the other wells using the same method except for the last two wells. One-hundred microliters of the solutions was discarded from one well after mixing, and the last well was used as negative control without adding any material. The concentration of log phase bacteria was adjusted to $1 \times 10^5$ CFU/mL by culture medium, and 10 μL bacterial suspension were added to each well, followed by incubation of the 96-well plates in a constant temperature oscillator at 30 °C for 24 h. Three replicates were prepared for each dose level. The turbidity of each well was observed, and the MIC of the drugs was determined by the transparent well corresponding to the lowest dose level.

**Persister Killing Test.** Previous studies have demonstrated that stationary-phase cells of *S.aureus* can be used to model persister


DOI: 10.1021/acsbiomaterials.9b00583
ACS Biomater. Sci. Eng. 2019, 5, 4739−4749

Scheme 2. Schematic Representation of the N-CQDs to Inactivate Bacteria and Disperse Biofilm

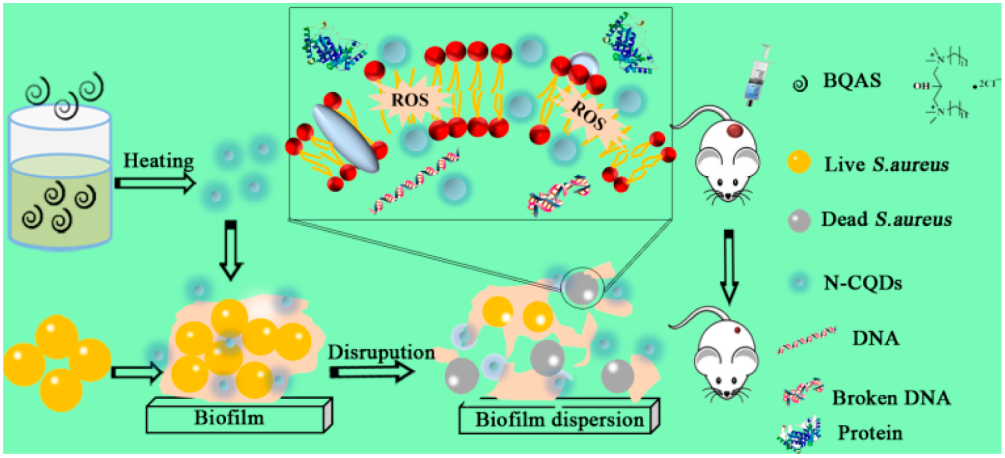


cells.[26] Briefly, persister cells of MRSA were prepared by growing cultures overnight to stationary phase at 37 °C at 225 rpm.[27] The obtained bacterial suspensions were washed before adjustment to 1−2 × $10^8$ CFU/mL with sterile water. After centrifugation, 500 μL of suspension was incubated with different concentrations of N-CQDs at 30 °C and 120 rmp. At specific time points (0, 45, 90,135, and 180 min), 100 μL samples were withdrawn, diluted to an appropriate concentration with sterile water, and spread on the LB agar plates. After incubation at 30 °C for 24 h, the colonies were counted to display the activity of N-CQDs against MRSA-persisters. These experiments were conducted in triplicate.

**Mature Biofilm Formation by MRSA.** To obtain mature biofilms, 10 μL of stationary phase MRSA bacterial suspension (1 × $10^7$ CFU/mL) and 990 μL of Tryptone Soy Broth (TSB) medium were added into 24-well microtiter plates, followed by culture at 37 °C to allow the formation of biofilm, with the medium renewed every 24 h.[28,29] After 48 h of incubation, each well was washed with PBS buffer to remove medium and unfixed bacteria under aseptic conditions.[30] Finally, biofilm could be seen clearly on the bottom of the well.

**Destruction of Biofilm by N-CQDs.** The destruction of biofilm was examined by crystal violet staining assay.[31] Briefly, The obtained biofilm of MRSA was incubated with a series of concentrations (0, 0.625, 1.25, 2.5 5, and 10 μg/mL) of N-CQDs for 24 h in TSB medium at 30 °C, followed by washing the remaining biofilms with PBS, adding crystal violet stain for 30 min, and eliminating the excess stain with PBS. Finally, the amount of the remaining biofilm stained by crystal violet was evaluated by adding 100% ethanol and measuring the optical absorbance at 590 nm.[32]

**Live/Dead Bacterial Staining Assay.** The viability of bacterial suspensions before and after treatment with N-CQDs was measured by the live/dead viability assay.[33,34] Briefly, after being treated with N-CQDs (30 °C, 3 h), the bacterial suspensions (200 μL, 1 × $10^8$ CFU/mL) were centrifugated, live/dead dye solution (30 μL of propidium iodide-PI and 30 μL if 4′-6-diamidino-2-phenylindole-DAPI) was added in the darkness for 30 min, 10 μL of the solution was then placed on a slide and covered with a coverslip, and it was finally imaged by a fluorescence microscopy. Bacteria treated with PBS was set up as control. The PI dye can only enter the structure (cell membrane)-damaged bacterial cells, stain the nucleus and then emit red fluorescence, while DAPI can pass through the intact membrane of cells, bind with DNA and then emit blue fluorescence. Hence, PI and DAPI were employed to indicate dead and live cells, respectively.[35] Meanwhile, the PI can explain the change of the permeability of cell membranes treated and untreated with N-CQDs. In addition, we used the image pro plus software to quantify the Live/Dead Bacterial Staining Assay.

**Morphology Study of Bacterial Cells.** The morphologies of bacterial cells before and after incubation with N-CQDs were observed by scanning electron microscopy (SEM, SIGMA-500) and transmission electron microscopy (TEM, JEM-2010 TEM), respectively. Briefly, after incubation with N-CQDs, the bacterial suspension (200 μL, $10^8$ CFU/mL) were washed twice with sterile water, followed by fixation with 0.5 mL of glutaraldehyde (2.5%) for 4 h at room temperature, and then, dehydration with 0.5 mL of ethanol gradient (30, 50, 70, 90 and 100%) for 15 min, respectively. Finally, SEM samples were prepared by drying the bacterial suspension at a vacuum freeze-dryer to obtain the bacterial powder, followed by coating the powder with gold by sputtering, then observed by SEM; TEM samples were prepared by placing one drop of the obtained bacterial suspension on the copper grids, then observed by TEM.

**Cytotoxicity Assay.** The cytotoxicity of the N-CQDs was carrired out via the MTT assay. Briefly, 4T1 cells were seeded in 96-well plates at 1 × $10^4$/well and cultured for 24 h at 37 °C under 5% $CO_2$. The cells were then treated with different concentrations (0.625, 1.25, 2.5, 5, 10, and 20 μg/mL) of N-CQDs and control DMEM (10% FBS) in triplicate for 4, 8, 12, and 24 h, separately. Afterward, 20 μL of MTT (3-[4,5- dimethylthiazol-2-thiazolyl]-2,5-diphenyl tetrazolium bromide) solution was added in each well, and the cells were further cultured for 4 h at 37 °C. After that, removed the supernatant in each well, and 150 μL of DMSO was finally added in each well to solubilize the formazan crystal. The absorbance was measured at 490 nm via employing an Enzyme Linked Immunosorbent Assay (ELISA) microplate reader.

**Lactase Dehydrogenase Release Test.** The cell membrane activity of bacteria incubated with N-CQDs was further tested by using the Cytotoxicity Detection $Kit^{PLUS}$ (LDH) according to the manufacturer's instructions (Roche Applied Science). Bacterial suspensions (200 μL, 1 × $10^8$ CFU/mL) were incubated with different concentrations (0.625, 1.25, 2.5, 5, 10, and 20 μg/mL) of N-CQDs for 3 h, followed by transferring 100 μL of culture supernatant from each cell to a new tube, adding substrate and well mixing. After incubation at room temperature in the dark for 1 h, the reaction was terminated by adding 50 μL of stop solution into the tubes. Bacteria treated with PBS as control. Finally, the release of the LDH was determined by examining the optical density at 490 nm.

**Leakage of Intracellular Components.** To further demonstrate the damage of the cell membrane, the release of protein in the bacterial cells treated with N-CQDs was tested by related experiments. We employed the Enhanced BCA Protein Assay Kit (Beyotime Shanghai). Briefly, first, 200 μL bacterial suspensions were centrifugated and then washed with PBS twice. Second, the obtained bacteria were treated with a series of concentrations (0.625, 1.25, 2.5, 5, 10, and 20 μg/mL) of N-CQDs for 3 h at 30 °C, bacteria treated with PBS under the same conditions was set up as control. Third, the suspensions were centrifugated (3000 r/min, 10 min) and the supernatant was used to examine the leakage of protein according to the instruction of the Enhanced BCA Protein Assay Kit. In addition, the supernatant was examined by SDS-PAGE (sodium dodecyl sulfate polyacrylamide gel electrophoresis).



DOI: 10.1021/acsbiomaterials.9b00583
ACS Biomater. Sci. Eng. 2019, 5, 4739−4749

**ROS Detection.** To assess the photocatalytic properties of N-CQDs, the electron spin resonance (ESR) spectroscopy was used to determine the reactive oxygen species (ROS) generated by N-CQDs employing 5,5-dimethyl-1-pyrroline-N-oxide (DMPO) as a capture agent. Briefly, the N-CQDs samples were added into 96-well plates, and then 100 $\mu$L of DMPO (100 mM) was added into the 96-well. Then, the samples were irradiated by visible light (300 W, 20 min), and finally, the ROS was measured by ESR spectroscopy (JES FA 200,JEOL Co.). N-CQDs without irradiated by visible light was established as control.

**In Vivo Mice Wound Model and Healing Process Analysis.** Animal experiments were conducted according to the Institutional Animal Care and Use Committee. To evaluate the antibacterial effect of N-CQDs in vivo, two different drug injection models (wound drop and tail vein injection) were built. Female BALB/c mice (6−8 weeks) were purchased and randomly divided into 4 groups: PBS, penicillin (Pen), vancomycin (Van), and N-CQDs. Treatments with PBS and Pen were used as blank and negative control, respectively. Each related experiment was repeated three times. Wounds were first obtained by injury on the back of the mice, and then infected with 100 $\mu$L ($1 \times 10^7$ CFU/mL) of MRSA suspensions separately. Twenty-four hours after infection, 100 $\mu$L (10 mg/kg) N-CQDs, Pen, Van, and PBS solutions were injected through tail vein or wound drop separately. The injection was carried out once per 24 h, with three consecutive injections. Photos of the wounds on the mice back from the four groups were taken at 0, 1, 3, and 7 days. Seven days later, all the mice were sacrificed to collect the wound tissues and all the wound tissues were fixed with formaldehyde solution (10%) for pathological slides. The histology analysis was performed using the Hematoxylin and Eosin (H&E) staining, and the collagen formation assessment was performed using the Masson's trichrome staining. In addition, the major organs (heart, liver, spleen, lung, and kidney) of mice from the four groups were collected after 7 days, then fixed with formaldehyde solution (10%) for H&E staining for preliminary toxicity analysis. Besides, the number of bacteria in the wound tissues was quantified at 0, 1, 3, and 7 days during the therapeutic process to show the antibacterial activity of N-CQDs. After the experiment, all the mice were handled according to the Institutional Animal Care and Use Committee.

**Statistical Analysis.** An independent $t$ test or one-way ANOVA test was used to analyze the experimental data. Data with error bars are expressed as the mean ± standard deviations. Statistical significance was determined with p value: $p < 0.05$ (*), $p < 0.01$ (**).

## RESULTS AND DISCUSSION

**Characterization of N-CQDs.** The morphology and structure of the as-prepared N-CQDs were investigated by employing a high-resolution transmission electron microscope (HRTEM). HRTEM result (Figure 1A) shows that nearly spherical N-CQDs with good dispersibility were successfully prepared, and the particles sizes was 2.15 ± 0.62 nm. The size distribution was confirmed by using DLS (Figure 1B), which is consistent with the result of HRTEM. The result of the stability of N-CQDs is displayed in Figure S2, it can be observed that there is no significant changes in particle size (~2 nm) at different times, which indicates the N-CQDs possess good stability in water. In addition, the results of FT-IR were presented in Figure 1C. The peaks at 3425 and 3236 $cm^{-1}$ were attributed to the stretching vibrations of N−H/O-H,the peaks at 2923 and 2850 cm-1 to C−H stretching, and peaks at 1618 cm-1 and 1140 cm-1 vibrations were assigned to N−H and C−OH bonds, the peak at 1465 cm-1 to C-NH bond.[36,37] Further, the chemical structure of N-CQDs was also studied by employing X-ray photoelectron spectroscopy (XPS). The XPS survey spectra (Figure 1D) indicates three peaks: C 1s at about 287.1 eV, O 1s at about 533.1 eV, and N 1s at about 403.1 eV, respectively. As shown in Figure 1D, The

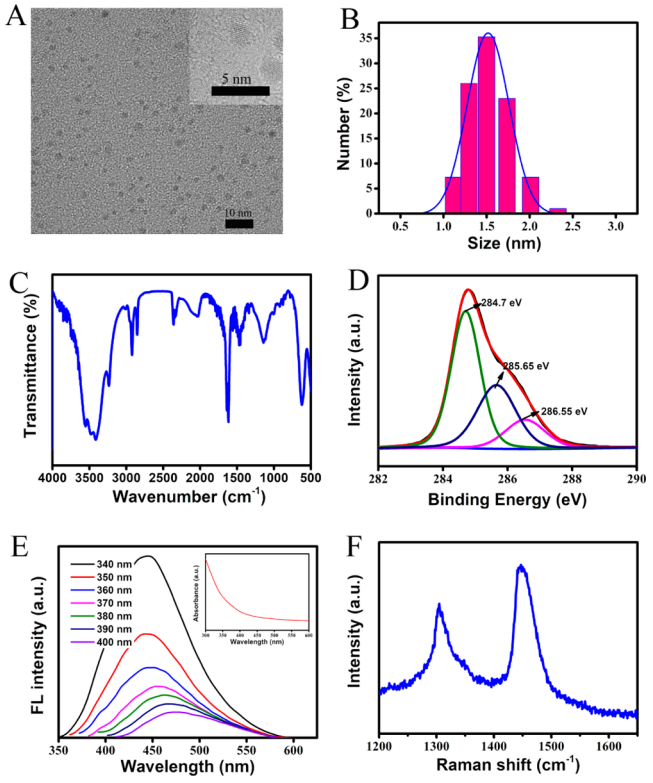


**Figure 1.** Characterization of N-CQDs. (A) HTEM images of N-CQDs. (B) Size distribution of N-CQDs measured by DLS. (C) FT-IR spectra, (D) XPS spectra, (E) photoluminescence spectra and UV−vis absorption spectra (the illustration), and (F) Raman spectrum of N-CQDs.

C 1s peak at 284.7, 285.65, and 286.55 eV confirmed the presence of C−C/C═C, C−N, and C−OH groups.[38,39] The chemical structure of N-CQDs determined by the XPS was in line with FT-IR results. The bulk composition of N-CQDs were analyzed by using the EA-IRMS (Table S1).The UV−vis absorption spectra of the N-CQDs in Figure. 1E shows that there was a wide absorption band in the absorption spectrum, which may be owing to the different size distribution of the N-CQDs.[40] The photoluminescence (PL) properties of the N-CQDs was studied. As shown in Figure. 1E, the emission wavelength shfit about 25 nm with the excitation wavelength increased (from 340 to 400 nm). The N-CQDs displayed an excitation-dependent FL behavior, which may be attributed to the presence of different particle sizes and a distribution of different emissive states of each particle.[41] Additionally, the zeta potential of N-CQDs was measured to be positively charged (ca. + 32 mV). Raman spectroscopy was also used to characterize the graphene structure of the obtained N-CQDs. As displayed in Figure 1F, Raman spectrum of the N-CQDs display two typical peaks at around 1305 and 1450 $cm^{-1}$, which means the N-CQDs possess both $sp^2$ (G-band) and $sp^3$ (D-band) hybrids. In addition, the coexistence of the two bands reveals that the N-CQDs are amorphous.[42]

**In Vitro Evaluation the Antimicrobial Activity of N-CQDs.** The antimicrobial activity of the cationic N-CQDs was assessed against several bacterial strains, including MRSA, ampicillin-resistant *E. coli*, *Staphylococcus aureus* (*S.aureus*), and *Escherichia coli* (*E. coli*). As shown in Table 1 and Figure S3, the N-CQDs showed a broad-spectrum antimicrobial activity toward all the microorganisms tested with low minimal


DOI: 10.1021/acsbiomaterials.9b00583
ACS Biomater. Sci. Eng. 2019, 5, 4739−4749

**Table 1. Minimal Inhibitory Concentrations of N-CQDs against Clinical MRSA and Standard Strains**

| microorganism | MIC ($\mu$g/mL) | | | | | |
|---|---|---|---|---|---|---|
| | N-CQDs | Van | Gen | Rfp | Pen | Meth |
| ampicillin-resistant *E.coli* | 8 | >64 | >64 | 4 | >64 | >64 |
| MRSA | 4 | 2 | 8 | 8 | >64 | >64 |
| *E.coli* (AB 93154) | 8 | 64 | 16 | 16 | 4 | 32 |
| *S.aureus* (AB 91093) | 2 | 2 | 4 | 8 | 4 | 32 |

inhibitory concentrations (MICs) compared with the five kinds of antibiotics (Van, vancomycin; Gen, gentamicin; Rfp, rifampin; Meth, methicillin; Pen, penicillin). The growth curve and death rate were evaluated for ampicillin-resistant *E. coli* and MRSA cells exposed to different concentrations of N-CQDs (Figure S4). It can be seen that with the increasing concentrations of N-CQDs (I-1−I-6 and II-1−II-6), the number of colonies decreased obviously on the plates, and when the cells were treated with 10 $\mu$g/mL of N-CQDs, the death rates reached almost 100%. These results showed that the N-CQDs possess excellent antibacterial capacity and the antibacterial activity is concentration-dependent.

With resistance development as a major concern, we assessed the ability of MRSA to develop resistance to N-CQDs. Serial passaging of MRSA in the presence of subinhibitory concentrations of such N-CQDs showed no detectable resistance to cationic N-CQDs (minimum inhibitory concentration (MIC) of 4 $\mu$g/mL at the first and twelfth passages), whereas the exposure of MRSA to the antibiotic RFP resulted in a rapid increase in MIC after five passages, and a $\geq$ 32-fold increase in MIC after eight passages (from 8 to >256 $\mu$g/mL; Figure 2A). In comparison with planktonic bacteria, biofilm-forming bacteria are tolerant owing to antibiotics fail to penetrate the thick biofilm, which make those bacteria more difficult to eradicate.[41,42]

In addition, biofilms are related to gene transfer between bacteria, which propagates antibiotic resistance.[43] Whether N-CQDs can hinder the formation of biofilms and eliminate biofilms were determined by related experiments. Figure 2B displays the effect of N-CQDs, Van, and Meth on the biofilms formation. It can be observed that compared with the groups treated with Van and Meth, the group treated with N-CQDs tends to decrease the biofilm formation rate in a concentration-dependent mode.

After exposure to the N-CQDs in the concentration range of 0−20 $\mu$g/mL for 24 h, the mature biofilm mass was examined by crystal violet staining. The results are displayed in Figure 2C and Figure S5. It can be seen that N-CQDs could obstruct and destroy the formation of biofilms of MRSA with a dose-dependent effect. When incubated with 1.25 $\mu$g/mL N-CQDs, about 16.7% of the biofilm mass was removed, and when incubated with 20 $\mu$g/mL N-CQDs, approximately 70% of the biofilm mass was eliminated. However, the destructive effect of Van and Meth on the mature biofilms were very weak and almost negligible.We also used fluorescent dyes to stain the living bacteria in the biofilm. The results are shown in Figure 2D, and the bacterial viability of biofilms decreased with increasing N-CQDs concentration, while the bacterial viability of biofilms treated with Van and Meth did not reduce, and the above results are in consistent with the results of crystal violet staining. In short, the obtained results suggest that N-CQDs possess the property of eliminating MRSA biofilms effectively.

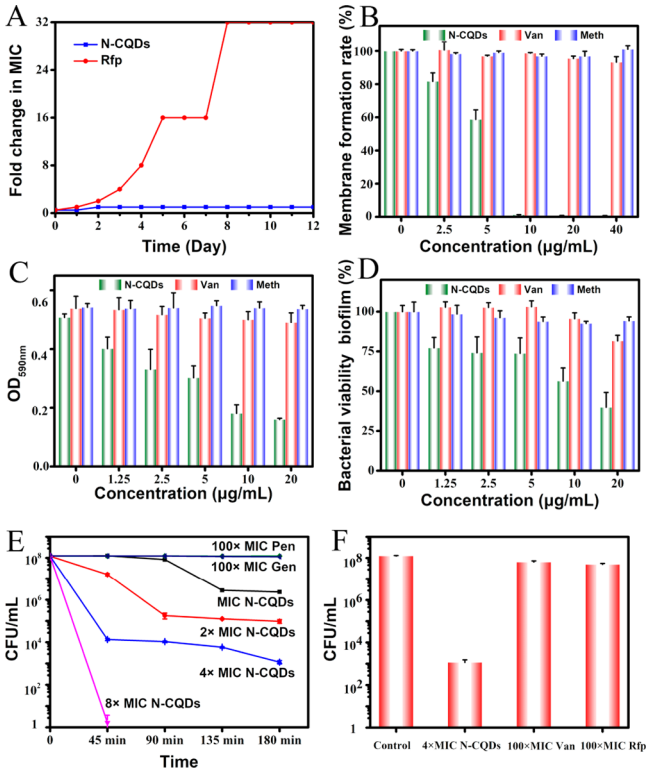


**Figure 2.** Antibacterial effect of N-CQDs against MRSA. (A) Development of drug resistance to N-CQDs and Rfp. (B) Efficacy of different concenrtations (0, 2.5, 5, 10, and 20 $\mu$g/mL) of the N-CQDs, Van, and Meth on the inhibition of MRSA biofilms. (C, D) Effect of different concenrtations of N-CQDs, Van, and Meth on the mature biofilms in MRSA model. (E) N-CQDs, Pen, and Gen were used to fight against persisters. Stationary-phase MRSA cells were treated with different concentrations of N-CQDs (MIC, 2 × MIC, 4 × MIC, and 8 × MIC) and 100× MIC conventional antibiotics. (F) Viability of stationary-phase MRSA cells when treated with the indicated concentrations of each material for 3 h. The error bars indicate means ± SD ($n$ = 3).

However, antibiotics cannot remove bacterial biofilms efficiently because they fail to penetrate the thick biofilms.[44,45]

Persisters, a kind of multidrug-tolerant bacterial cells ubiquitous among bacterial species, are considered to be responsible for the recalcitrance of many bacterial infections to antibiotic treatment and have a role in the relapse and recalcitrance of infections.[46] Additionally, persisters are related to the increased risk of the emergence and spread of traditional antibiotic resistance.[44] The emergence of antibiotic-resistant bacteria and bacterial persisters are two huge challenges for treating bacterial infections. Further more, we examined the ability of N-CQDs in killing MRSA persisters. *S. aureus* readily forms persisters, which are nongrowing dormant cells and many antibiotic target sites are inactive, therefore resulting in a high level of tolerance to most traditional antibiotics.[47,48]

The activity of N-CQDs against persisters was assessed by exposing the biofilms of MRSA to different concentrations of N-CQDs (MIC, 2 × MIC, 4 × MIC, and 8 × MIC) and high-dose antibiotics of Pen and Gen (100× MIC) for a series of time points (0, 45, 90, 135, and 180 min). The results showed that the 8 × MIC N-CQDs could completely eradicate MRSA-persister cells (Figure 2E) within 45 min, while the antibiotics (Pen and Gen) at a concentration of 100 × MIC showed no inhibition effect even after 4 h treatment. Figure 2F displays



DOI: 10.1021/acsbiomaterials.9b00583
ACS Biomater. Sci. Eng. 2019, 5, 4739−4749

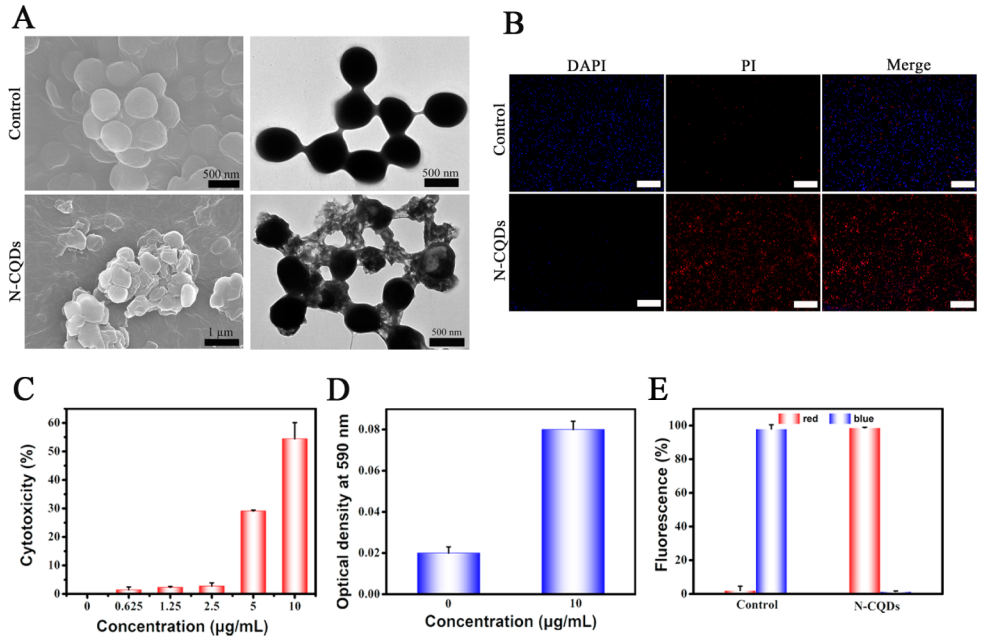


**Figure 3.** N-CQDs combat the bacteria via a multipath mechanism. (A) Typical SEM images (left panel) and TEM images (right panel) showing the morphological changes of MRSA ($1 \times 10^8$ CFU/mL) treated in the absence (upper panel) or presence (down panel) of N-CQDs (10 $\mu$g/mL) for 3 h at 30 °C. (B) Fluorescence microscope images of MRSA ($1 \times 10^8$ CFU/mL) untreated (upper panel) and treated (down panel) with N-CQDs (10 $\mu$g/mL) for 3 h at 30 °C after staining with PI and DAPI (scale bars: 50 $\mu$m) (C) Characterization of the integrity of bacterial membrane determined by the cytotoxicity measured by LDH release from the MRSA cells after treatment with different concentrations of N-CQDs (0, 0.625, 1.25, 2.5, 5, and 10 $\mu$g/mL) for 3 h at 30 °C, and (D) the protein leakage (determined at OD 590 nm) of MRSA suspensions treated with or without N-CQDs (10 $\mu$g/mL) for 3 h at 30 °C. (E) The corresponding measurement of live/dead fluorescence of MRSA. The error bars indicate means ± SD ($n$ = 3).

the survival rate of bacteria, with 4 × MIC N-CQDs killing over 90% persisters, and 100 × MIC Van and Rfp killing only a few persisters. These results indicate that N-CQDs have a good eradication effect against the MRSA-persister cells.

**Antibacterial Mechanism of N-CQDs toward MRSA.** The antibacterial mechanism of N-CQDs was explored using MRSA and Ampicillin-resistant *E. coli* as the model bacteria. We observed the morphological changes of MRSA and Ampicillin-resistant *E. coli* treated with N-CQDs by SEM and TEM. Compared with the control (upper panel), MRSA cells treated with 10 $\mu$g/mL N-CQDs (down panel) became wrinkled and collapse, implying the disruption of membrane integrity (Figure 3A) induced by N-CQDs.

Besides, N-CQDs induced the membrane injury that was further visualized via the live/dead staining assay with PI and DAPI (Figure 3B). After staining, a large area of blue fluorescence (live cell) and only a small amount of red fluorescence (dead cell) are observed in the control group, suggesting the cells are alive and the membrane is intact. In contrast, we can see almost all bacteria treated with N-CQDs display red fluorescence, and hardly any blue fluorescence can be seen, implying N-CQDs lead to the destruction of membrane and the death of bacteria. In addition, N-CQDs showed the same effect on the membrane of ampicillin-resistant *E. coli* (Figures S6 and S7A), and the corresponding quantitative flourescence data are shown in Figure 3E (MRSA) and Figure S7B (ampicillin-resistant *E. coli*); we can see that the results are in line with the previous results.

The morphological changes of the structure of bacterial cells after treatment with N-CQDs could be ascribed to the detachment of the cytoplasmic membrane from the cell wall, which was examined by the extent of cell damage quantitatively determined using the LDH release assay. Figure 3C and Figure S8A exhibit the LDH activity in the supernatant of bacterial cells (MRSA and Ampicillin-resistant *E. coli*, respectively) after incubation with a serise of concentrations of N-CQDs for 3 h. As expected, a concentration-dependent LDH release was expressed when bacterial cells were incubated with N-CQDs. The bacterial cells treated with 0.625 $\mu$g/mL of N-CQDs exhibited the minimal LDH release; however, when treated with 10 $\mu$g/mL of N-CQDs, the LDH release significantly increased, reaching 54.44% and 60.41% of MRSA and ampicillin-resistant *E. coli*, respectively. In short, N-CQDs significantly affect the bacterial cell membrane integrity, which subsequently resulted in the release of the cell contents. The disruption of the structure and the increased permeability of bacterial cell membrane induced by N-CQDs were also verified by the release of cytoplasmatic content (protein). The results are displayed in Figure 3D and Figure S8B, C. As shown in Figure S8B, there were clear strips in lanes 1 and 3, which represented the proteins of the supernatants of ampicillin-resistant *E. coli* and MRSA treated with N-CQDs, respectively, whereas there was no strip in lanes 2 and 4 for bacterial cells untreated with N-CQDs. We used Enhanced BCA Protein Assay Kit to determine the released protein. The absorbance at 590 nm (OD590 nm) reflects the level of the leaked protein (MRSA). As shown in Figure 3D and Figure S8C, the treatment of N-CQDs significantly increased the release of protein, destroyed the cell membranes of both MRSA and ampicillin-resistant *E. coli*, and increased their permeability. These results are consistent with the aforementioned experiments.

Furthermore, we investigated the biochemical processes triggered by N-CQDs when in contact with the bacteria. ROS,


DOI: 10.1021/acsbiomaterials.9b00583
ACS Biomater. Sci. Eng. 2019, 5, 4739−4749

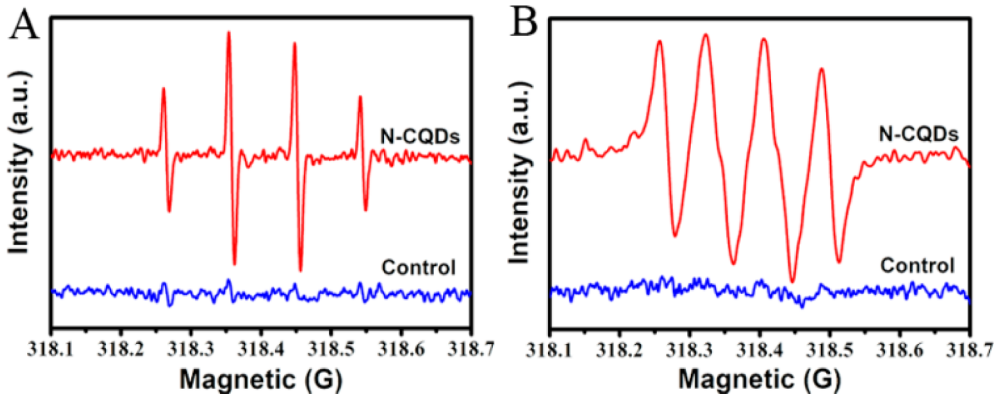


**Figure 4.** ESR images of (A) DMPO-·OH and (B) DMPO-·O2- for N-CQDs under irradiation. ROS was identified by ESR spectroscopy.

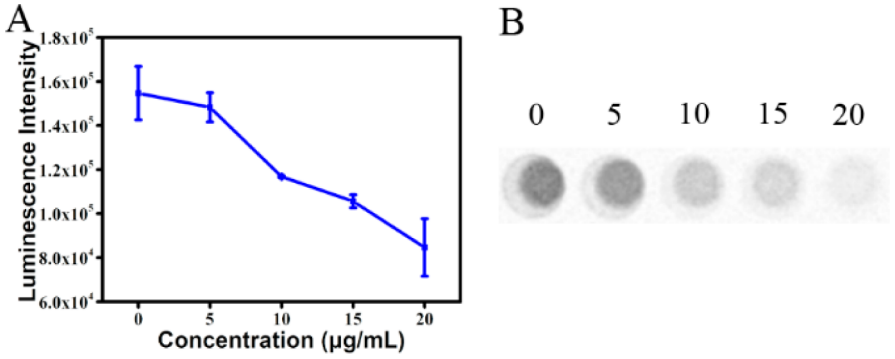


**Figure 5.** Intracellular ATP level of MRSA (200 $\mu$L, 1 × $10^8$ CFU/mL) treated with different concentrations of N-CQDs (0, 5, 10, 15, and 20 $\mu$g/mL) for 3 h at 30 °C. Error bars represent the standard deviation of three repeated measurements.

especially the hydroxyl radical (•OH) and singlet oxygen ($O_2^1$) are reported to induce the damage of cell membranes, protein, and DNA, and then lead to the death of bacteria.[49−53] To determine whether N-CQDs can also generate ROS, we conducted the ROS measurements by ESR at room temperature. DMPO (100 mM) was used to trap •OH and $O_2^1$ under visible light irradiation, and the results are shown in Figure 4. As expected, N-CQDs did generate •OH (Figure 4A) and $•O^{2-}$ (Figure 4B), which can cause damage to cellular membrane, intracellular proteins, and DNA. The effect of N-CQDs on DNA was tested by using the plasmid DNA of *E. coli*. As shown in Figure S9A, the brightness of the strips varies with the concentrations of N-CQDs. With the concentration of N-CQDs increased, the brightness of the band became weaker or even disappeared, indicating that N-CQDs induce the degradation of plasmid DNA of *E. coli*.

Considering the crucial role of the surface-chemical properties of nanoparticles in the interaction with cells, the effect of the surface-chemical properties of N-CQDs on their antibacterial activity was investigated by measuring their charges. The N-CQDs were found to be positively charged (ca. + 32 mV), whereas the surface of bacterial cells is known to be negatively charged, and previous studies have suggested that the positive charge contributes to the increased membrane permeability and ultimately the damage of the bacterial membrane.[54] In this study, when bacterial cells were exposed to N-CQDs, a strong electrostatic interaction is induced between them, followed by the disruption of the membrane structure of bacterial cells. To further confirm the influence of surface charge on the antibacterial capacity of N-CQDs, we prepared N-CQDs containing 10 $\mu$M BSA with a $\zeta$-potential of ca. + 10 mV (Figure S9B) and evaluated the antibacterial activity of the positively charged N-CQDs (ca.+32 mV) and the N-CQDs supplemented with BSA (ca.+10 mV) at the same concentration using the MRSA model. The results are presented in Figure S9C. It can be observed that adding BSA obviously decreased the antibacterial activity of N-CQDs. Additionally, the MIC of the N-CQDs added with BSA (10 $\mu$M) was 16 $\mu$g/mL, which was larger than the pure N-CQDs at the same concentration. The above results implied that the positive charges of N-CQDs contributed to their antibacterial property, which because the positive charges favored the strong electrostatic interaction between N-CQDs and the membrane of bacterial cells, and then help to wreck the integrity of the cell membrane/well, resulting in the release of intracellular contents and the death of bacterial cells. Additionally, the impact of N-CQDs on bacterial metabolism was assessed by measuring the intracellular ATP levels (ATP Assay Kit), and the results are shown in Figure 5. It displays the intuitive effect of N-CQDs on the amount of intracellular ATP, with the color of the spots fading, suggesting that the ATP level decreases. Figure 5A shows the ATP level as measured by the value of luminescence intensity. It can be observed that, with the concentrations of N-CQDs increased, the chemiluminescence signal value became smaller, which meant the ATP level reduced. The results demonstrated that N-CQDs did obstruct the bacterial metabolism to some extent.

**Compatibility of N-CQDs.** The compatibility of N-CQDs were examined using an MTT cytotoxity assay. As displayed in Figure S10, the viability of 4T1 cells is more than 90% within 20 $\mu$g/mL of N-CQDs after coculturing for 4, 8, and 12 h, separately. In addition, after coculturing for 24 h, the N-CQDs


DOI: 10.1021/acsbiomaterials.9b00583
ACS Biomater. Sci. Eng. 2019, 5, 4739−4749

show little toxicity to 4T1 cells and the viability of 4T1 cells is close to 73%, hence, N-CQDs possess good compatibility.

**In Vivo Evaluation the Antimicrobial Activity of N-CQDs.** The antibacterial activity of N-CQDs in vivo was evaluated by using two different drug injection models. Figures 6 and 7 display the results of antibacterial activity by tail vein injection. To assess the antibacterial activity, we researched the wound area and survival bacteria in the wounds (Figure 6 and Figure S11). The wound photographs at 0, 1, 3, 5, and 7 days are displayed in Figure 6A. Compared with groups of the control and Pen, the wounds area in the groups of N-CQDs and Van are reduced obviously after 3 days. After 7 days, obvious scabs are observed from the control and Pen group. In contrast, the wounds are smaller than that of in the N-CQDs and Van group, indicating a better recovery in the N-CQDs and Van group. Figure 6C shows the wound area, we can see that the wound area decreases with time, especially the wound in the group of N-CQDs, hence, the N-CQDs can furnish better wound closure than control group and Pen, but the difference is not signifcant between N-CQDs and Van, which suggested that the antibacterial activity of N-CQDs is as good as Van.

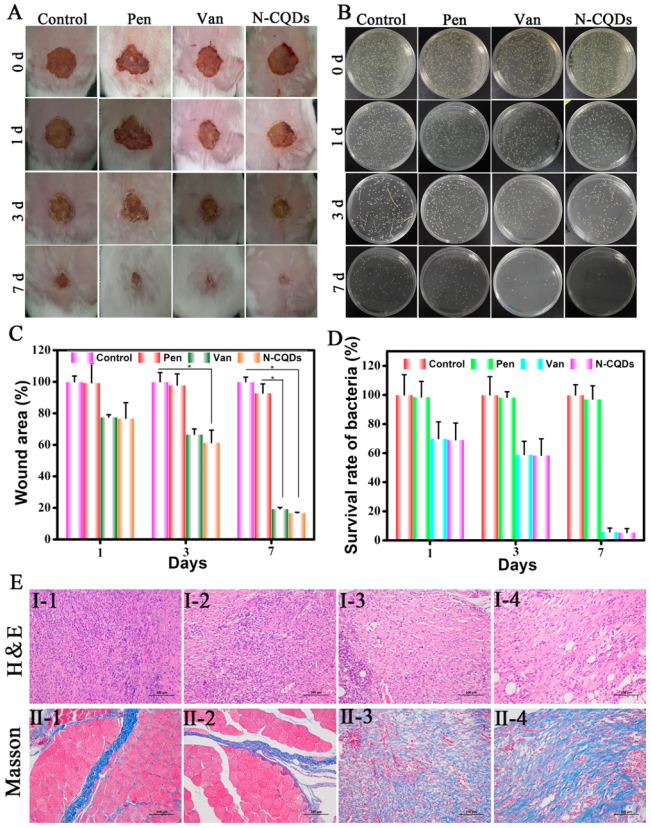


**Figure 6.** In vivo demonstration of N-CQDs in accelerating infectious wound healing. (A) Photographs of wounds and (B) LB-agar plate images of surviving bacteria at 0, 1, 3, and 7 days. (C) Wound area from the four groups at different time points during the therapeutic process. (D) Survival rate of bacteria in the wound. (E) H&E staining (I-1−I-4) and Masson trichrome staining (II-1−II-4) of the wounds in the different treatment groups. I-1−I-4/II-1−II-4: PBS, Pen, Van, and N-CQDs. Results are presented as the mean ± SD ($n$ = 3): $p$ < 0.05 (*) and $p$ < 0.01(**).

Besides, the number of bacteria in the wound tissues were counted after collected the tissues. The results are presented in Figure 6B, compared with the control group, the number of colony forming units (CFU) in the Pen group remained almost unchanged, whereas the CFU in groups treated with N-CQDs and Van obviously decreased. Figure 6D shows the corresponding quantitative statistics of bacterial survival rate. After 7 days, the bacterial survival rate decreases to 5% in the N-CQDs group, corresponding to the antibacterial effect in the Van group. Additionally, the therapeutic effects were evaluated by histological analysis. The wounds in the BALB/C mice were harvested after the treatment of 7 days and then exposed to H&E staining and Masson trichrome staining. Infected tissues tended to generate neutrophils, which were stained in blue. Figure 6E(I-1−I-4) displays the results of H&E staining. It can be observed that the N-CQDs group (I-4) as well as the Van group (I-3) show similar staining results (less blue area). In contrast, more blue area can be observed in the PBS (I-1) and Pen group (I-2), indicating that the wound tissues were seriously infected. The results demonstrate that the wound healing effect is almost the same between N-CQDs and Van. Besides, Masson's trichrome staining was utilized to evaluate the formation of collagen fiber (blue) during the process of the wound healing.

The results are shown in Figure 6E(II-1−II-4). It can be seen obviously that there is less blue area presented in the groups of PBS (II-1) and Pen (II-2) but more blue area in the groups of N-CQDs (II-3) and Van (II-4). Blue represents collagen fibers; therefore, the results indicate that connective tissues were formed in the wounds treated with N-CQDs, which is a good signal of skin regeneration and wound healing.

Figure S10 exhibits the antibacterial results of N-CQDs by wound drop, and a similar result can be obtained. Briefly, after treatment with different conditions (PBS, Pen, Van, and N-CQDs), both of the bacterial inhibition rate and the wound healing area rate in the group of N-CQDs is similar to that of the group of Van but larger than that of in the groups of PBS and Pen. The H&E staining shows less blue area (neutrophils) in the group of N-CQDs and Van; the Masson's trichrome staining shows that the connective tissues formed in the group of N-CQDs is more obvious than that in the groups of PBS and Pen. Therefore, it can be concluded that N-CQDs shows good antibacterial activity in vivo.

In vivo organ system toxicity of N-CQDs was also examined. The major organs of mice (heart, lung, liver, spleen, and kidney) were harvested after 7 d, and histology analysis was performed. The results are displayed in Figure 7, it can be observed that the treatment with N-CQDs expressed negligible organ damage compared with the control, suggesting the safety of N-CQDs as a potential therapeutic agent. But if people want to replace antibiotics by N-CQDs in clinical applications, it needs more research, for example, long-term toxicity, to ensure the safety of N-CQDs to human.

## CONCLUSIONS

In summary, we successfully synthesized the environmentally friendly cationic carbon quantum dot nanoparticles by a simple method. The nanoparticles are capable of preventing biofilm formation and eliminating established biofilm and persister cells, and more importantly, they do not induce resistance to MRSA. In vivo results also comfirm that the N-CQDs have a better antibacterial activity than the other known antibiotics (such as vancomycin and gentamicin). The excellent bactericidal activity is attributed to the strong interaction between N-CQDs and bacterial membrane, which leads to the


DOI: 10.1021/acsbiomaterials.9b00583
ACS Biomater. Sci. Eng. 2019, 5, 4739−4749

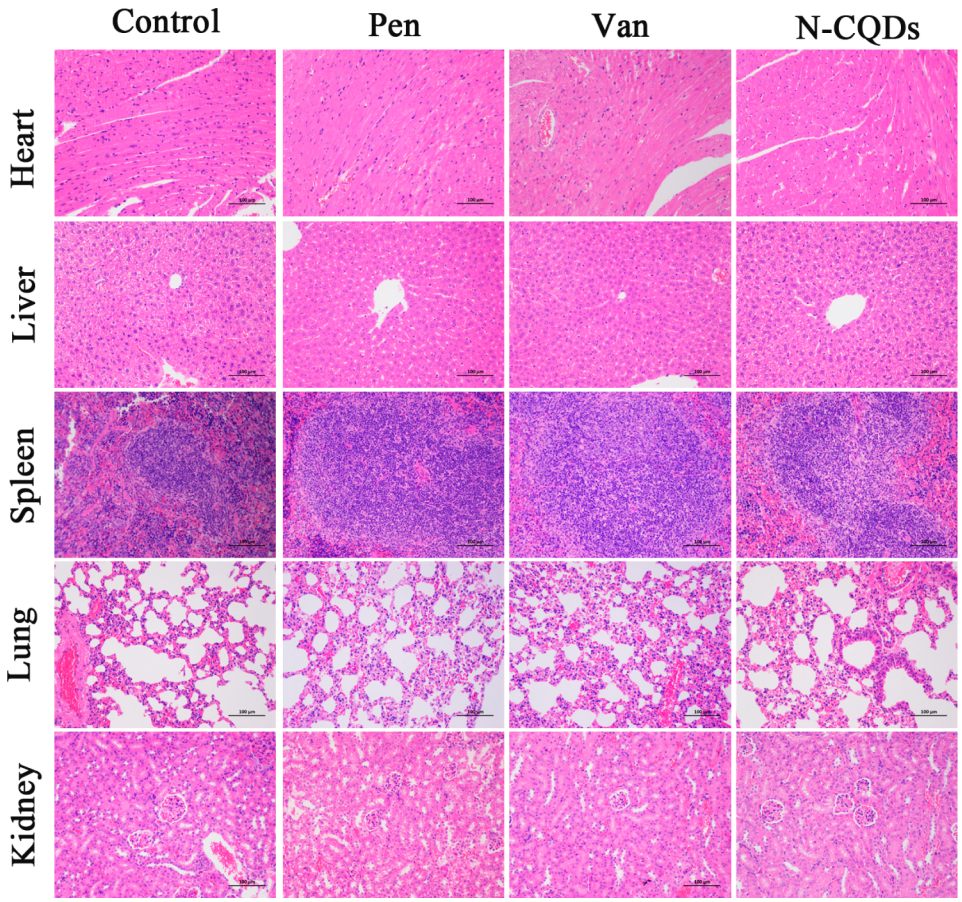


**Figure 7.** Preliminary toxicity analysis of N-CQDs: H&E staining images of the major organs (heart, liver, spleen, lung, and kidney) of MRSA-infected mice obtained by sliced for H&E staining after 7 days for toxicological observation.

damage and the increased permeability of the bacterial membrane as well as the release of intracellular contents. Additionally, ROS generated by N-CQDs can induce irreversible damage to nucleic acids and proteins, and N-CQDs can disrupt the metabolism of bacterial cells in a degree. All these factors ultimately result in the death of bacterial cells. Our findings provide new insights into the application of N-CQDs in the antibacterial field. The excellent antibacterial activity of N-CQDs suggest their potential as a green antibiotic in treating bacterial infections.

## ■ ASSOCIATED CONTENT

### Supporting Information

The Supporting Information is available free of charge on the ACS Publications website at DOI: 10.1021/acsbiomaterials.9b00583.

Figures S1−S11 (PDF)

## ■ AUTHOR INFORMATION

### Corresponding Author

*Email: hyhan@mail.hzau.edu.cn.

### ORCID

Zhiyong Song: 0000-0002-2552-5239
Jiangjiang Gu: 0000-0002-5161-2571
Heyou Han: 0000-0001-9406-0722

### Author Contributions

†H.W. and Z.S. contributed equally. The manuscript was written through contributions of all authors. All authors have given approval to the final version of the manuscript.

### Notes

The authors declare no competing financial interest.

## ■ ACKNOWLEDGMENTS

The authors are grateful to the financial support by the National Natural Science Foundation of China (21778020, 21807036), the Fundamental Research Funds for the Central Universities (2662016QD027), Sci-tech Innovation Foundation of Huazhong Agriculture University (2662017PY042, 2662018PY024). We are also thankful to Prof. Hanchang Zhu for editing of the language.

## ■ REFERENCES

(1) Flemming, H. C.; Wingender, J. The Biofilm Matrix. *Nat. Rev. Microbiol.* **2010**, *8*, 623−633.
(2) Olsen, I. Biofilm-Specific Antibiotic Tolerance and Resistance. *Eur. J. Clin. Microbiol. Infect. Dis.* **2015**, *34*, 877−886.
(3) Anderl, J. N.; Franklin, M. J.; Stewart, P. S. Role of Antibiotic Penetration Limitation in *Klebsiella pneumonise* Biofilm Resistance to Ampicillin and Ciprofloxacin. *Antimicrob. Agents Chemother.* **2000**, *44*, 1818−1824.
(4) Stewart, P. S.; Costerton, J. W. Antibiotic Resistance of Bacteria in Biofilms. *Lancet* **2001**, *358*, 135−138.
(5) de Breij, A.; Riool, M.; Cordfunke, R. A.; Malanovic, N.; de Boer, L.; Koning, R. I.; Ravensbergen, E.; Franken, M.; van der Heijde, T.;



DOI: 10.1021/acsbiomaterials.9b00583
*ACS Biomater. Sci. Eng.* 2019, 5, 4739−4749

Boekema, B. K.; Kwakman, P. H. S.; Kamp, N.; El Ghalbzouri, A.; Lohner, K.; Zaat, S. A. J.; Drijfhout, J. W.; Nibbering, P. H. The Antimicrobial Peptide SAAP-148 Combats Drug-Resistant Bacteria and Biofilms. *Sci. Transl. Med.* **2018**, *10*, eaan4044−4058.
(6) Ling, L. L.; Schneider, T.; Peoples, A. J.; Spoering, A. L.; Engels, I.; Conlon, B. P.; Mueller, A.; Schäberle, T. F.; Hughes, D. E.; Epstein, S.; Jones, M.; Lazarides, L.; Steadman, V. A.; Cohen, D. R.; Felix, C. R.; Fetterman, K. A.; Millett, W. P.; Nitti, A. G.; Zullo, A. M.; Chen, C.; Lewis, K. A New Antibiotic Kills Pathogens without Detectable Resistance. *Nature* **2015**, *517*, 455−459.
(7) Conlon, B. P.; Nakayasu, E. S.; Fleck, L. E.; LaFleur, M. D.; Isabella, V. M.; Coleman, K.; Leonard, S. N.; Smith, R. D.; Adkins, J. N.; Lewis, K. Activated ClpP Kills Persisters and Eradicates a Chronic Biofilm Infection. *Nature* **2013**, *503*, 365−370.
(8) Huh, A. J.; Kwon, Y. J. Nanoantibiotics": A New Paradigm for Treating Infectious Diseases Using Nanomaterials in the Antibiotics Resistant Era. *J. Controlled Release* **2011**, *156*, 128−145.
(9) Mukherjee, D.; Zou, H. X.; Liu, S. P.; Beuerman, R.; Dick, T. Membrane-targeting AM-0016 Kills Mycobacterial Persisters and Shows Low Propensity for Resistance Development. *Future Microbiol.* **2016**, *11*, 643−650.
(10) Chen, X.; Zhang, M.; Zhou, C. H.; Kallenbach, N. R.; Ren, D. C. Control of Bacterial Persister Cells by Trp/Arg Containing Antimicrobial Peptides. *Appl. Environ. Microbiol.* **2011**, *77*, 4878−4885.
(11) Blair, J. M. A.; Webber, M. A.; Baylay, A. J.; Ogbolu, D. O.; Piddock, L. J. V. Molecular mechanisms of antibiotic resistance. *Nat. Rev. Microbiol.* **2015**, *13*, 42−51.
(12) Vestergaard, M.; Paulander, W.; Marvig, R. L.; Clasen, J.; Jochumsen, N.; Molin, S.; Jelsbak, L.; Ingmer, H.; Folkesson, A. Antibiotic combination therapy can select for broad-spectrum multidrug resistance in Pseudomonas aeruginosa. *Int. J. Antimicrob. Agents* **2016**, *47*, 48−55.
(13) Tamma, P. D.; Cosgrove, S. E.; Maragakis, L. L. Combination therapy for treatment of infections with gram-negative bacteria. *Clin. Microbiol. Rev.* **2012**, *25*, 450−470.
(14) Brown, E. D.; Wright, G. D. Antibacterial drug discovery in the resistance era. *Nature* **2016**, *529*, 336−343.
(15) Aruguete, D. M.; Kim, B.; Hochella, M. F.; Ma, Y. J.; Cheng, Y. W.; Hoegh, A.; Liu, J.; Pruden, A. Antimicrobial Nanotechnology: Its Potential for the Effective Management of Microbial Drug Resistance and Implications for Research Needs in Microbial Nanotoxicology. *Environ. Sci.: Processes Impacts* **2013**, *15*, 93−102.
(16) Zhao, C.; Deng, B.; Chen, G. C.; Lei, B.; Hua, H.; Peng, H. L.; Yan, Z. M. Large-Area Chemical Vapor Deposition-Grown Monolayer Graphene-wrapped Silver Nanowires for Broad-spectrum and Robust Antimicrobial Coating. *Nano Res.* **2016**, *9*, 963−973.
(17) Black, C. L. K.; Sileika, T. S.; Yi, J.; Zhang, R.; Rivera, J. G.; Messersmith, P. B. Bacterial Killing by Light-Triggered Release of Silver from Biomimetic Metal Nanorods. *Small* **2014**, *10*, 169−178.
(18) Xu, X. Y.; Ray, R.; Gu, Y. L.; Ploehn, H. J.; Gearheart, L.; Raker, K.; Scrivens, W. A. Electrophoretic Analysis and Purification of Fluorescent Single-Walled Carbon Nanotube Fragments. *J. Am. Chem. Soc.* **2004**, *126*, 12736−12737.
(19) Li, H. T.; Kang, Z. H.; Liu, Y.; Lee, S. T. Carbon Nanodots: Synthesis, Properties and Applications. *J. Mater. Chem.* **2012**, *22*, 24230−24253.
(20) Thakur, M.; Pandey, S.; Mewada, A.; Patil, V.; Khade, M.; Goshi, E.; Sharon, M. Antibiotic Conjugated Fluorescent Carbon Dots as A Theranostic Agent for Controlled Drug Release, Bioimaging, and Enhanced Antimicrobial Activity. *J. Drug Delivery* **2014**, *2014*, 282193−282201.
(21) Lim, S. Y.; Shen, W.; Gao, Z. Q. Carbon Quantum Dots and Their Applications. *Chem. Soc. Rev.* **2015**, *44*, 362−381.
(22) Bing, W.; Sun, H.; Yan, Z.; Ren, J.; Qu, X. Programmed Bacteria Death Induced by Carbon Dots with Different Surface Charge. *Small* **2016**, *12*, 4713−4718.
(23) Wang, L. S.; Gupta, A.; Rotello, V. M. Nanomaterials for the Treatment of Bacterial Biofilms. *ACS Infect. Dis.* **2016**, *2*, 3−4.
(24) Li, X. N.; Yeh, Y. C.; Giri, K.; Mout, R.; Landis, R. F.; Prakash, Y. S.; Rotello, V. M. Control of Nanoparticle Penetration into Biofilms through Surface Design. *Chem. Commun.* **2015**, *51*, 282−285.
(25) Xie, Y. Z. Y.; Liu, Y.; Yang, J. C.; Liu, Y.; Hu, F. P.; Zhu, K.; Jiang, X. Y. Gold Nanoclusters for Targeting Methicillin-Resistant *Staphylococcus aureus* in Vivo. *Angew. Chem., Int. Ed.* **2018**, *57*, 3958−3962.
(26) Conlon, B. P.; Rowe, S. E.; Gandt, A. B.; Nuxoll, A. S.; Donegan, N. P.; Zalis, E. A.; Clair, G.; Adkins, J. N.; Cheung, A. L.; Lewis, K. Persister Formation in *Staphylococcus aureus* is Associated with ATP Depletion. *Nat. Microbiol.* **2016**, *1*, 16051.
(27) Brown, E. D.; Wright, G. D. Antibacterial drug discovery in the resistance era. *Nature* **2016**, *529*, 336−343.
(28) Sun, H. J.; Gao, N.; Dong, K.; Ren, J. S.; Qu, X. G. Graphene Quantum Dots-Band-Aids Used for Wound Disinfection. *ACS Nano* **2014**, *8*, 6202−6210.
(29) Bing, W.; Chen, Z.; Sun, H.; Shi, P.; Gao, N.; Ren, J.; Qu, X. Visible-light-driven enhanced antibacterial and biofilm elimination activity of graphitic carbon nitride by embedded Ag nanoparticles. *Nano Res.* **2015**, *8*, 1648−1658.
(30) Amorena, B.; Gracia, E.; Monzón, M.; Leiva, J.; Oteiza, C.; Pérez, M.; Alabart, J. L.; Yago, J. H. J. Antibiotic Susceptibility Assay for *Staphylococcus aureus* in Biofilms Developed in vitro. *J. Antimicrob. Chemother.* **1999**, *44*, 43−55.
(31) Duan, F.; Feng, X. C.; Jin, Y.; Liu, D. W.; Yang, X. J.; Zhou, G. Q.; Liu, D. D.; Li, Z. H.; Liang, X. J.; Zhang, J. C. Metal−Carbenicillin Framework-Based Nanoantibiotics with Enhanced Penetration and Highly Efficient Inhibition of MRSA. *Biomaterials* **2017**, *144*, 155−165.
(32) Barraud, N.; Kardak, B. G.; Yepuri, N. R.; Howlin, R. P.; Webb, J. S.; Faust, S. N.; Kjelleberg, S.; Rice, S. A.; Kelso, M. J. Cephalosporin-3′-diazeniumdioates: Targeted NO-Donor Prodrugs for Dispersing Bacterial Biofilms. *Angew. Chem., Int. Ed.* **2012**, *51*, 9057−9060.
(33) Wu, M. C.; Deokar, A. R.; Liao, J. H.; Shih, P. Y.; Ling, Y. C. Graphene-Based Photothermal Agent for Rapid and Effective Killing of Bacteria. *ACS Nano* **2013**, *7*, 1281−1290.
(34) Sun, L.; Du, T.; Hu, C.; Chen, J. N.; Lu, J.; Lu, Z. C.; Han, H. Y. Antibacterial Activity of Graphene Oxide/g-C3N4 Composite through Photocatalytic Disinfection under Visible Light. *ACS Sustainable Chem. Eng.* **2017**, *5*, 8693−8701.
(35) Chen, J. N.; Peng, H.; Wang, X. P.; Shao, F.; Yuan, Z. D.; Han, H. Y. Graphene Oxide Exhibits Broad-Spectrum Antimicrobial Activity against Bacterial Phytopathogens and Fungal Conidia by Intertwining and Membrane Perturbation. *Nanoscale* **2014**, *6*, 1879−1889.
(36) Jia, Z.; Xu, W. Synthesis and Antibacterial Activities of Quaternary Ammonium Salt of Chitosan. *Carbohydr. Res.* **2001**, *333*, 1−6.
(37) Du, T.; Liang, J. G.; Dong, N.; Liu, L.; Fang, L. R.; Xiao, S. B.; Han, H. Y. Carbon Dots as Inhibitors of Virus by Activatiob of Type I Interferon Response. *Carbon* **2016**, *110*, 278−285.
(38) Chen, W. F.; Li, D. J.; Tian, L.; Xiang, W.; Wang, T. Y.; Hu, W. M.; Hu, Y. L.; Chen, S. N.; Chen, J. F.; Dai, Z. X. Synthesis of Graphene Quantum Dots from Natural Polymer Starch for Cell Imaging. *Green Chem.* **2018**, *20*, 4438−4442.
(39) Zhang, H.; Chen, Y.; Liang, M.; Xu, L.; Qi, S.; Chen, H.; Chen, X. Solid-Phase Synthesis of Highly Fluorescent Nitrogen-Doped Carbon Dots for Sensitive and Selective Probing Ferric Ions in Living Cells. *Anal. Chem.* **2014**, *86*, 9846−9852.
(40) Zhou, J. G.; Booker, C.; Li, R. Y.; Zhou, X. T.; Sham, T. K.; Sun, X. L.; Ding, Z. F. An electrochemical avenue to blue luminescent nanocrystals from multiwalled carbon nanotubes (MWCNTs). *J. Am. Chem. Soc.* **2007**, *129*, 744−745.
(41) Zhou, J. J.; Sheng, Z. H.; Han, H. Y.; Zou, M. Q.; Li, C. X. Facile synthesis of fluorescent carbon dots using watermelon peel as a carbon source. *Mater. Lett.* **2012**, *66*, 222−224.
(42) Liu, R. L.; Wu, D. Q.; Liu, S. H.; Koynov, K.; Knoll, W.; Li, Q. An Aqueous Route to Multicolor Photoluminescent Carbon Dots


DOI: 10.1021/acsbiomaterials.9b00583
*ACS Biomater. Sci. Eng.* 2019, 5, 4739−4749

Using Silica Spheres as Carriers. *Angew. Chem.* **2009**, *121*, 4668−4671.
(43) Du, J.; Bandara, H. M. H. N.; Du, P.; Huang, H.; Hoang, K.; Nguyen, D.; Mogarala, S. V.; Smyth, H. D. C. Improved Biofilm Antimicrobial Activity of Polyethylene Glycol Conjugated Tobramycin Compared to Tobramycin in *Pseudomonas aeruginosa* Biofilms. *Mol. Pharmaceutics* **2015**, *12*, 1544−1553.
(44) Mu, H.; Tang, J.; Liu, Q.; Sun, C.; Wang, T.; Duan, J. Potent Antibacterial Nanoparticles Against Biofilm and Intracellular Bacteria. *Sci. Rep.* **2016**, *6*, 18877−18885.
(45) Molin, S.; Nielsen, T. T. Gene Transfer Occurs with Enhanced Efficiency in Biofilms and Induces Enhanced Stabilisation of the Biofilm Structure. *Curr. Opin. Biotechnol.* **2003**, *14*, 255−261.
(46) Du, J.; Bandara, H. M. H. N.; Du, P.; Huang, H.; Hoang, K.; Nguyen, D.; Mogarala, S. V.; Smyth, H. D. C. Improved biofilm antimicrobial activity of polyethylene glycol conjugated tobramycin compared to tobramycin in pseudomonas aeruginosa biofilms. *Mol. Pharmaceutics* **2015**, *12*, 1544−1553.
(47) Gerdes, K.; Semsey, S. Microbiology: Pumping Persisters. *Nature* **2016**, *534*, 41.
(48) Keren, I.; Kaldalu, N.; Spoering, A.; Wang, Y.; Lewis, K. Persister Cells and Tolerance to Antimicrobials. *FEMS Microbiol. Lett.* **2004**, *230*, 13−18.
(49) Allison, K. R.; Brynildsen, M. P.; Collins, J. J. Metabolite-Eabled Eradication of Bacterial Persisters by Aminoglycosides. *Nature* **2011**, *473*, 216−220.
(50) Kim, W.; Fricke, N.; Conery, A. L.; Fuchs, B. B.; Rajamuthiah, R.; Jayamani, E.; Vlahovska, P. M.; Ausubel, F. M.; Mylonakis, E. NH125 Kills Methicillin-Rsistant *Staphylococcus aureus* Persisters by Lipid Bilayer Disruption. *Future Med. Chem.* **2016**, *8*, 257−269.
(51) Li, Y.; Liu, X. M.; Tan, L.; Cui, Z. D.; Yang, X. J.; Zheng, Y. F.; Yeung, K. W. K.; Chu, P. K.; Wu, S. L. Rapid Sterilization and Accelerated Wound Healing Using Zn2+ and Graphene Oxide Modified g-C3N4 under Dual Light Irradiation. *Adv. Funct. Mater.* **2018**, *28*, 1800299−1800310.
(52) Tian, X.; Jiang, X. M.; Welch, C.; Croley, T. R.; Wong, T. Y.; Chen, C.; Fan, S. H.; Chong, Y.; Li, R. B.; Ge, C. C.; Chen, C. Y.; Yin, J. J. Bactericidal Effects of Silver Nanoparticles on Lactobacilli and the Underlying Mechanism. *ACS Appl. Mater. Interfaces* **2018**, *10*, 8443−8450.
(53) Applerot, G.; Lipovsky, A.; Dror, R.; Perkas, N.; Nitzan, Y.; Lubart, R.; Gedanken, A. Enhanced Antibacterial Activity of Nanocrystalline ZnO Due to Increased ROS-Mediated Cell Injury. *Adv. Funct. Mater.* **2009**, *19*, 842−852.
(54) Liu, H.; Du, Y. M.; Wang, X. H.; Sun, L. P. Chitosan Kills Bacteria through Cell Membrane Damage. *Int. J. Food Microbiol.* **2004**, *95*, 147−155.


DOI: 10.1021/acsbiomaterials.9b00583
*ACS Biomater. Sci. Eng.* 2019, 5, 4739−4749